Aspects of diffraction of a creeping wave by a back-wall crack

V Zernov, L Fradkin, A Gautesen, Michel Darmon

Journal of Physics: Conference Series **353** (2012) 012017 doi:10.1088/1742-6596/353/1/012017

Aspects of diffraction of a creeping wave by a back-wall crack

V Zernov[1], L Fradkin[1], A Gautesen[2] and M Darmon[3]

[1] Sound Mathematics Ltd., Cambridge, CB4 2AS, UK
[2] Dept. of Mathematics, Iowa State University and Ames Laboratory, Ames, IA 50011, U. S. A.
[3] CEA, LIST, 91191 Gif-sur-Yvette CEDEX, France.

E-mail: v.zernov@soundmathematics.com

Abstract. In this paper we address the issue of a creeping wave by investigating a two-dimensional configuration which involves a surface-braking crack in a traction free planar back-wall. We assume that this back-wall is irradiated by a shear Gaussian beam which is incident at a critical angle and hits the wall away from the crack edge. We show that the generated wave - known in the engineering literature as "creeping", because it propagates near the surface - consists of non-geometrical waves, the longitudinal and transverse components of the head wave and a longitudinal Goodier-Bishop type wave whose amplitude grows linearly with the distance to its propagation path. The "creeping" wave interacts with the crack edge but the resulting field cannot be simulated using the Kirchhoff Approximation, because this does not embrace the higher order effects. We show that the diffracted field can be simulated using a modification of the Uniform Geometrical Theory of Diffraction which involves a relatively simple limiting procedure.

1. Introduction

Interaction of an ultrasonic beam with a surface-breaking planar faces crack is a well known problem in NDE (Non-Destructive Evaluation). Two-dimensional configurations in which a beam irradiates the whole crack can be modelled using the UGDT as developed for diffraction by half-planes and wedges [1], [2], [3]. In this paper we study an even more challenging problem of scatter of a high frequency Gaussian beam by a crack whose edge lies outside the beam - see Fig. 1. In the engineering literature this situation is usually referred to as interaction between a crack and "creeping wave" that the beam generates. There are several high-frequency approximations which offer effective computational algorithms for many scattering problems. The simplest and most versatile among those is the Kirchhoff Approximation which is based on the Geometrical Elastodynamics. However the Geometrical Elastodynamics is correct only to the leading order and cannot be used to describe the next order effects. For this reason the Kirchhoff approximation fails when the incident transversal beam hits the inspection surface at an angle close to critical. In this paper we show how to conduct efficient simulations of the above configuration using a simple modification of another well-known high-frequency approximation, the Geometrical Theory of Diffraction (GTD). First we develop approximations to the field generated by the incident beam near the wall - the "creeping" wave - because it is only this field that interacts with the crack edge. The paper is organised as follows: In Section 2 we introduce the problem, first assuming the incident field to be a cylindrical wave and then generalising that to a Gaussian beam, which is a good approximation to a realistic transducer beam. In Section 3, we use a near boundary approximation to show that the scattered "creeping" wave can be described as a combination of the T (transverse) portion of the head wave, its L (longitudinal) portion propagating along the

surface and a somewhat unusual L wave whose amplitude grows proportionally to the distance to the path of propagation The latter is known in the literature as a Goodier-Bishop wave [4]. In Section 4 we justify a limiting procedure that allows us to use a canonical GTD problem of plane wave diffraction by a wedge to simulate wedge diffraction of the "creeping" wave. In Section 5 we present numerical results and in Section 6, discussion of some controversial issues. We finish by describing what has been achieved and issues that require further consideration.

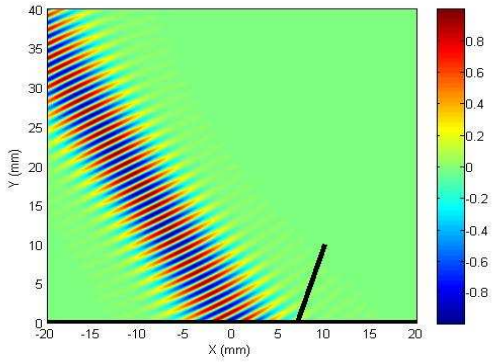

Figure 1. A back-wall crack (solid black line) irradiated by a Gaussian beam.

2. The problem statement

We consider an isotropic and homogeneous elastic medium occupying a half-space and assume a two-dimensional configuration, with the associated Cartesian basis $\{\mathbf{e}_1, \mathbf{e}_2\}$ such that $\mathbf{e}_1$ runs along the boundary, $\mathbf{e}_2$ is its inner normal and the third axis is implied but omitted everywhere below. Therefore all points $\boldsymbol{x}$ referred to below lie in the same plane and are characterised only by two coordinates x_1 and x_2. If the circular frequency is ω, then whatever time harmonic displacement field $\boldsymbol{u}\exp(i\omega t)$ is excited inside this medium, its amplitude $\boldsymbol{u} = \boldsymbol{u}(\boldsymbol{x})$ can be written in terms of the longitudinal potential $\phi = \phi(\boldsymbol{x})$ and transverse potential $\psi = \psi(\boldsymbol{x})$,

$$\boldsymbol{u} = \nabla\phi + \nabla^{\perp}\psi, \tag{1}$$

where the nabla operators are $\nabla = (\partial_1, \partial_2)$, $\nabla^{\perp} = (\partial_2, -\partial_1)$ and ∂_i is a symbol of partial differentiation with respect to the spatial coordinate x_i, $i = 1, 2$. Everywhere below we use the following nomenclature: a field is designated by superscript $^{\text{creep}}$, $^{\text{GB}}$, $^{\text{H}}$, $^{\text{inc}}$, $^{\text{ref}}$, $^{\text{scat}}$ or $^{\text{tot}}$ to indicate whether it is creeping, Goodier-Bishop type, head, incident, reflected, scattered or total wave, respectively. Note that the words "scattered field" are used to describe a combination of diffracted and reflected fields. One section below introduces a concept of a remainder field and utilises the subscript $^{\text{rem}}$ explained there. The accompanying subscript describes the nature of the incidence $_{\text{cyl}}$, $_{\text{plane}}$ and $_{\text{Gauss}}$ for cylindrical wave, plane wave and Gaussian beam, respectively. In addition, when describing displacement fields this subscript also includes letters $_L$, $_T$ and $_C$ for longitudinal, transverse and creeping waves, respectively. In the absence of body forces, the total potentials satisfy the following Helmholtz equations

$$\Delta\phi^{\text{tot}} + k_L^2\phi^{\text{tot}} = 0, \quad \Delta\psi^{\text{tot}} + k_T^2\psi^{\text{tot}} = 0, \tag{2}$$

where the Laplacian $\Delta = \partial_1^2 + \partial_2^2$, $k_\alpha = \omega/c_\alpha$, $\alpha = L, T$, with k_L,k_T,c_L and c_T - the wave numbers and speeds of the longitudinal (L) and transverse (T) waves, respectively. Let $\sigma^{\text{tot}} = \{\sigma_{ij}^{\text{tot}}\}$ be the amplitude of the related stress tensor,

$$\sigma_{ij}^{\text{tot}}(\boldsymbol{u}) = \lambda\delta_{ij}\nabla\cdot\boldsymbol{u}^{\text{tot}} + \mu\left(u_{i,j}^{\text{tot}} + u_{j,i}^{\text{tot}}\right), \quad i, j = 1, 2, \tag{3}$$

where λ and μ are the Lamé constants, and the comma before an index denotes differentiation with respect to the corresponding spatial coordinate, so that e.g. $u_{i,j} = \partial_j u_i$. Then the traction free boundary condition can be written as

$$\sigma_{12}^{\rm tot}|_{x_2=0} = \sigma_{22}^{\rm tot}|_{x_2=0} = 0. \tag{4}$$

We impose the usual radiation condition at infinity and assume that a line source $-Ck_T^{-2}\delta(x_1 - a_1)\delta(x_2 - a_2)$ running through a point $\boldsymbol{a} = (a_1, a_2)$ excites transverse potential $\psi_{\rm cyl}^{\rm inc}(\boldsymbol{x})$. It is well known that the above incident potential is proportional to the outward propagating cylindrical function, Hankel function of the first kind,

$$\psi_{\rm cyl}^{\rm inc}(\boldsymbol{x}) = \frac{{\rm i}C}{4k_T^2} H_0^{(1)}\left(k_T r\right), \tag{5}$$

where $r = \sqrt{(x_1 - a_1)^2 + (x_2 - a_2)^2}$ is the distance from observation point to excitation source. Let us now present the coordinates a_1 and a_2 in the form

$$a_1 = a\cos\varphi^{\rm inc}, \quad a_2 = a\sin\varphi^{\rm inc}, \tag{6}$$

where φ is the polar angle associated with the Cartesian coordinates (x_1, x_2). Let us allow the distance a from the source to the coordinate origin to be complex, with $\operatorname{Im} a \geq 0$. Let us further introduce an auxiliary Cartesian coordinate system (x_1', x_2') with the origin at $(\operatorname{Re} a\cos\varphi^{\rm inc}, \operatorname{Re} a\sin\varphi^{\rm inc})$ and the axis x_1' running in the direction of vector $(\cos\varphi^{\rm inc}, \sin\varphi^{\rm inc})$. Then the incident cylindrical wave turns into a Gaussian beam,

$$\psi_{\rm Gauss}^{\rm inc}(\boldsymbol{x}) = \frac{{\rm i}C}{4k_T^2} H_0^{(1)}\left(k_T r\right) \approx \frac{{\rm i}C}{4k_T^2}\sqrt{\frac{2}{{\rm i}\pi k_T r}}\,{\rm e}^{k_T\left[\operatorname{Im} a - \frac{(x_2')^2}{2\omega^2}\right]}\,{\rm e}^{{\rm i}k_T\left[x_1' + \frac{(x_2')^2}{2\rho}\right]}, \ |k_T r| \gg 1, \tag{7}$$

where the beam radius of curvature ϱ and beam spot size w are given, respectively, by

$$\varrho = x_1'\left[1 + \left(\frac{\operatorname{Im} a}{x_1'}\right)^2\right], \quad w^2 = \operatorname{Im} a\left[1 + \left(\frac{x_1'}{\operatorname{Im} a}\right)^2\right]. \tag{8}$$

Below we impose the condition

$$C = {\rm e}^{-\operatorname{Im} a k_T} \tag{9}$$

and assume that the incident field is a Gaussian beam. We choose this type of incidence, because it is a good approximation to a realistic transducer beam and because it allows for an analytical treatment. To simplify our calculations, we introduce the double Fourier transform

$$\widetilde{f}(\boldsymbol{\xi}) = \int_{-\infty}^{+\infty}\int_{-\infty}^{+\infty} f{\rm e}^{-{\rm i}(\xi_1 x_1 + \xi_2 x_2)}dx_1 dx_2, \tag{10}$$

where $\boldsymbol{\xi} = (\xi_1, \xi_2)$ is an arbitrary wave vector, and also the single Fourier transform in x_1

$$\widehat{f}(\xi_1, x_2) = \int_{-\infty}^{+\infty} f{\rm e}^{-{\rm i}\xi_1 x_1}dx_1. \tag{11}$$

Introducing the line source into the right hand side of the second equation in (2) and applying to it the double Fourier transform, $\widetilde{\psi}_{\rm cyl}^{\rm inc}(\boldsymbol{\xi})$ satisfies the following algebraic equation:

$$(k_T^2 - \xi_1^2 - \xi_2^2)\widetilde{\psi}(\boldsymbol{\xi}) = -Ck_T^{-2}{\rm e}^{-{\rm i}\xi_1 a_1}{\rm e}^{-{\rm i}\xi_2 a_2} \tag{12}$$

and therefore its inverse Fourier transform in ξ_2 is

$$\widehat{\psi}^{\rm inc}_{\rm cyl}(\xi_1,x_2)=\frac{C{\rm e}^{-{\rm i}\xi_1 a_1}}{2\pi k_T^2}\int_{-\infty}^{+\infty}\frac{{\rm e}^{{\rm i}\xi_2(x_2-a_2)}}{\xi_2^2-\eta_T^2}d\xi_2. \tag{13}$$

Above and below we use the notation

$$\eta_\alpha=\sqrt{k_\alpha^2-\xi_1^2},\ \alpha=L,\,T. \tag{14}$$

As explained in the Introduction, we are interested only in the total field near the traction-free boundary. Imposing the corresponding condition, the integral in (13) can be evaluated on the basis of the Cauchy Residue Theorem, provided the contour of integration is distorted to pass the pole $\xi_2=\eta_T$ from below and $\xi_2=-\eta_T$ from above. It can be shown that provided ${\rm Im}\,a_2=0$ or the Gaussian beam is not grazing the back-wall, under the source $({\rm Re}\,a_1,{\rm Re}\,a_2)$

$$\widehat{\psi}^{\rm inc}_{\rm Gauss}(\xi_1,x_2)=\frac{{\rm i}C}{2\eta_T k_T^2}{\rm e}^{-{\rm i}[\xi_1 a_1+\eta_T(x_2-a_2)]},\quad x_2<{\rm Re}\,a_2. \tag{15}$$

3. Interaction of the shear Gaussian beam with the traction-free planar surface

The Helmholtz equations (1) are satisfied, respectively, by both the total potentials $\phi^{\rm tot}_{T({\rm Gauss})}=\phi^{\rm scat}_{T({\rm Gauss})}$, $\psi^{\rm tot}_{T({\rm Gauss})}=\psi^{\rm inc}_{\rm Gauss}+\psi^{\rm scat}_{T({\rm Gauss})}$ and incident potential $\psi^{\rm inc}_{\rm Gauss}$. Therefore they are satisfied by the potential $\phi^{\rm scat}_{T({\rm Gauss})}$ which is scattered by the medium boundary. Applying the Fourier transform in x_1 to (1) we obtain ordinary differential equations of the second order. This means that the Fourier transforms in x_1 of the scattered (outgoing) potentials that satisfy the radiation condition at infinity have the form

$$\widehat{\phi}^{\rm scat}_{T({\rm Gauss})}(\xi_1,x_2)=R_{TL}\widehat{\psi}^{\rm inc}_{\rm Gauss}(\xi_1,0){\rm e}^{{\rm i}\eta_L x_2},\quad \widehat{\psi}^{\rm scat}_{T({\rm Gauss})}(\xi_1,x_2)=R_{TT}\widehat{\psi}^{\rm inc}_{\rm Gauss}(\xi_1,0){\rm e}^{{\rm i}\eta_T x_2}. \tag{16}$$

Substituting (16) into the boundary condition (4) which is first re-formulated for the scattered potentials and is then Fourier transformed in x_1 gives us the reflection coefficients R_{TL} and R_{TT},

$$R_{TL}=-\frac{2\bar\eta_T^2\eta_T\xi_1}{\mathcal{R}(\xi_1)},\ R_{TT}=-\frac{\bar{\mathcal{R}}(\xi_1)}{\mathcal{R}(\xi_1)}, \tag{17}$$

where $\bar\eta_T=\sqrt{k_T^2/2-\xi_1^2}$ and the Rayleigh function $\mathcal{R}$ and its conjugate $\bar{\mathcal{R}}$ are given by

$$\mathcal{R}(\xi_1)=\bar\eta_T^4+\xi_1^2\eta_L\eta_T,\ \ \bar{\mathcal{R}}(\xi_1)=\bar\eta_T^4-\xi_1^2\eta_L\eta_T. \tag{18}$$

The expressions for scattered elastodynamic potentials $\widehat{\phi}^{\rm scat}_T$ and $\widehat{\psi}^{\rm scat}_T$ which are valid near the traction-free planar surface can be found by applying the inverse Fourier transform in ξ_1 to (15) and (16), respectively. We perform this operation in the next subsections.

3.1. The scattered T component of the head wave - a near surface approximation

It is well known that a ray incident on the plane at a critical angle gives rise to a head wave (see [5] and references therein). The T portion of the head wave can be described by a contribution to the T component of the inverse Fourier transform in ξ_1 of a branch point in η_L. Let us start this calculation by rewriting R_{TT} as

$$R_{TT}=-\frac{{\rm i}C}{2k_T^2\eta_T}\left(\frac{\bar\eta_T^8+\xi_1^4\eta_L^2\eta_T^2}{\bar\eta_T^8-\xi_1^4\eta_L^2\eta_T^2}-\eta_L\frac{2\xi_1^2\bar\eta_T^4\eta_T}{\bar\eta_T^8-\xi_1^4\eta_L^2\eta_T^2}\right){\rm e}^{{\rm i}(-\xi_1 a_1+\eta_T a_2)}. \tag{19}$$

Only the second term contains a branch point at $\eta_L = 0$. The corresponding part of the inverse Fourier transform is

$$\psi^H_{T(\text{Gauss})} = \frac{\mathrm{i}C}{k_T^2}\int_{-\infty}^{\infty} \eta_L \frac{\xi_1^2\bar{\eta}_T^4}{\bar{\eta}_T^8 - \xi_1^4\eta_L^2\eta_T^2}\mathrm{e}^{\mathrm{i}[\xi_1(x_1-a_1)+\eta_T(a_2+x_2)]}d\xi_1. \tag{20}$$

Provided the distance to the boundary is small, $k_T x_2 \approx 0$, this potential can be shown to be

$$\psi^H_{T(\text{Gauss})} = \frac{E_c}{(k_L d_1)^{3/2}}\psi^0, \quad \psi^0 = \frac{4\mathrm{i}\gamma\mathrm{e}^{\mathrm{i}(k_L x_1 + k_T \sin\varphi^{head} x_2)}}{k_T(2\gamma^2-1)}, \tag{21}$$

where the critical angle $\varphi^{\text{head}} = \cos^{-1}\gamma$, the distance d_1 is defined graphically in Fig. 2 and the constant E_c is given by

$$E_c = \frac{\sqrt{2\pi\mathrm{i}}\,C\gamma^3}{k_T(2\gamma^2-1)}\mathrm{e}^{\mathrm{i}(-k_L a_1 + k_T\sqrt{1-\gamma^2}a_2)}. \tag{22}$$

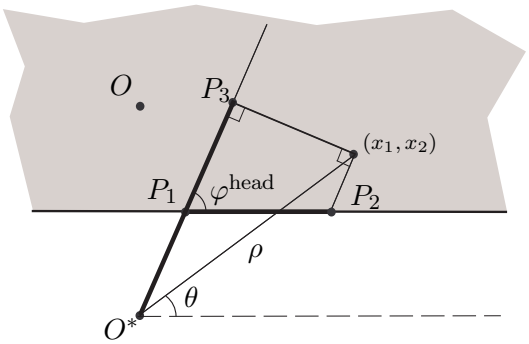

Figure 2. Geometry associated with the scattered T wave. $O = (\mathrm{Re}\,a_1, \mathrm{Re}\,a_2)$ - the point source, $O^* = (\mathrm{Re}\,a_1, -\mathrm{Re}\,a_2)$ the imaginary source, (x_1, x_2) - the observation point. $d_0 = O^*P_3$, $d_1 = P_1P_2$.

3.2. The scattered L waves - a near surface approximation

Combining (16) and (17) and applying the inverse Fourier transform in ξ_1, the scattered longitudinal potential is

$$\phi^{\text{scat}}_{T(\text{Gauss})} = -\frac{\mathrm{i}C}{k_T^2}\int_{-\infty}^{\infty}\frac{\xi_1\bar{\eta}_T^2}{\mathcal{R}(\xi_1)}\mathrm{e}^{\mathrm{i}[\xi_1(x_1-a_1)+\eta_T a_2+\eta_L x_2]}d\xi_1. \tag{23}$$

Let us assume that the observation point lies far from the point where the axis of the incident Gaussian beam hits the boundary $k_L\widetilde{d} \gg 1$, where the distance $\widetilde{d}$ is defined graphically in Fig. 3). It can be shown that in this approximation, we have

$$\phi^{\text{creep}}_{T(\text{Gauss})} = \frac{\sqrt{2\pi\mathrm{i}}C\gamma^2\mathrm{e}^{\mathrm{i}\Phi(\widetilde{\vartheta})}}{k_T^2}\left[\frac{A(\widetilde{\vartheta})}{(k_L\widetilde{d})^{1/2}} - \frac{\mathrm{i}A''(\widetilde{\vartheta})}{2(k_L\widetilde{d})^{3/2}}\right] + O\left((k_L\widetilde{d})^{-5/2}\right), \tag{24}$$

where

$$A(\widetilde{\vartheta}) = \frac{2\widetilde{\vartheta}}{1-2\gamma^2} + O(\widetilde{\vartheta}^2), \quad A''(\widetilde{\vartheta}) = -\frac{16\gamma^3\sqrt{1-\gamma^2}}{(1-2\gamma^2)^3} + O(\widetilde{\vartheta}) \tag{25}$$

and the angle $\widetilde{\vartheta}$ is defined graphically in Fig. 3. Then near the boundary $\widetilde{d\vartheta} \approx x_2$ and we obtain

$$\phi^{\text{creep}}_{T(\text{Gauss})} = \frac{E_c}{(k_L\widetilde{d})^{3/2}}\phi^0, \quad \phi^0 = -\left[\frac{8\mathrm{i}\gamma^3\sqrt{1-\gamma^2}}{k_L(1-2\gamma^2)^2} + 2x_2\right]\mathrm{e}^{\mathrm{i}k_L x_1}, \tag{26}$$

where the coefficient E_c is defined by (22). It follows that the longitudinal component is a sum of two waves, one ordinary and another - the Goodier-Bishop type wave whose amplitude grows linearly with the distance to its propagation path [4].

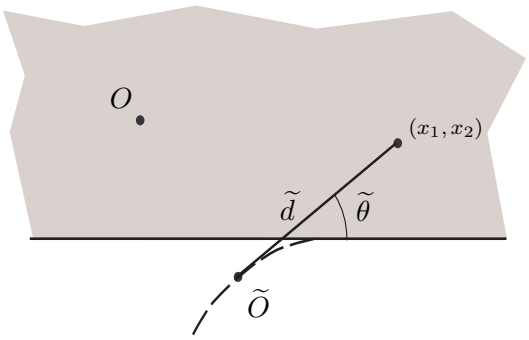

Figure 3. Geometry associated with the scattered L wave. $O = (\mathrm{Re}\, a_1, \mathrm{Re}\, a_2)$ - the point source, $\widetilde{O} = (\mathrm{Re}\,\widetilde{a}_1, \mathrm{Re}\,\widetilde{a}_2)$ - an imaginary L source. Dashed line - locus of imaginary sources for the observation angles $\widetilde{\vartheta}$ that vary between 0 to $\pi/2$.

4. Interaction of the "creeping" wave with a planar faces crack

Let us now assume that the back-wall contains an infinite planar surface-breaking crack. Formulae (21) and (26) show that near the boundary the field generated by an incident shear Gaussian beam and known as the "creeping" wave consists of one T wave and two L waves. If this combination reaches a crack before its amplitude becomes negligible the interference between resulting reflected and diffracted waves creates patches of significant amplitude. In this paper we concentrate on diffraction of the "creeping" wave and in order to calculate its amplitude we first investigate an auxiliary problem of diffraction of a plane L wave.

Let the incident L wave

$$\boldsymbol{u}^{\text{inc}}_{L(\text{plane})} = \frac{1}{\mathrm{i}k_L}\nabla\mathrm{e}^{\mathrm{i}k_L(x_1\cos\vartheta_L - x_2\sin\vartheta_L)}, \tag{27}$$

irradiate the crack and let the angle it forms with the face ($x_2 = 0+$, $x_1 < 0$) be near grazing, $\vartheta_L \approx 0$. In the second quadrant ($x_1 \le 0$, $x_2 \ge 0$) the resulting total field can be written as

$$\boldsymbol{u}^{\text{tot}}_{L(\text{plane})} = \boldsymbol{u}^{\text{inc}}_{L(\text{plane})} + \boldsymbol{u}^{\text{ref}}_{L(\text{plane})} + \boldsymbol{u}^{\text{rem}}_{L(\text{plane})}. \tag{28}$$

where $\boldsymbol{u}^{\text{ref}}_{L(\text{plane})}$ is the sum of the first reflected L and T waves and $\boldsymbol{u}^{\text{rem(aux)}}$ is the remainder. The reflected term is

$$\boldsymbol{u}^{\text{ref}}_{L(\text{plane})} = \frac{R_{LL}}{\mathrm{i}k_L}\nabla\mathrm{e}^{\mathrm{i}k_L(x_1\cos\vartheta_L + x_2\sin\vartheta_L)} + \frac{R_{LT}}{\mathrm{i}k_T}\nabla^{\perp}\mathrm{e}^{\mathrm{i}k_T(x_1\cos\vartheta_T + x_2\sin\vartheta_T)}, \tag{29}$$

where R_{LL} and R_{LT} are the respective reflection coefficients [8] and the angle ϑ_T is determined by the Snell's law, $k_L\cos\vartheta_L = k_T\cos\vartheta_T$. For $\vartheta_L \ll 1$ these reflection coefficients, can be expanded in $\vartheta_L \ll 1$ to give

$$R_{LL} = -1 + \frac{8\gamma^3\sqrt{1-\gamma^2}}{(1-2\gamma^2)^2}\vartheta_L + O(\vartheta_L^2), \quad R_{LT} = \frac{4\gamma}{(1-2\gamma^2)}\vartheta_L + O(\vartheta_L^2). \tag{30}$$

As $\vartheta_L \to 0$, $R_{LL} \to -1$ and $R_{LT} \to 0$ and the sum of the first two terms in (28) - which in the grazing limit becomes the field incident on the crack - vanishes,

$$\lim_{\vartheta_L \to 0} \left(\boldsymbol{u}^{\text{inc}}_{L(\text{plane})} + \boldsymbol{u}^{\text{ref}}_{L(\text{plane})} \right) = 0. \tag{31}$$

Since the wedge diffraction problem has an unique solution this implies

$$\lim_{\vartheta_L \to 0} \boldsymbol{u}^{\text{rem}}_{L(\text{plane})} = 0. \tag{32}$$

It follows that as $\vartheta_L \to 0$ diffraction coefficients $D_{L\beta}(\vartheta_L; \vartheta), \beta = L, T$ vanish too, that is, we have

$$\lim_{\vartheta_L \to 0} D_{L\beta}(\vartheta_L; \vartheta) = 0, \beta = L, T. \tag{33}$$

for all observation angles ϑ.

To proceed, we note that there is a simple relation between the normalised creeping waves described in the previous section

$$\boldsymbol{u}^{\text{inc}}_0 \equiv \nabla \phi^0 + \nabla^{\perp} \psi^0 \tag{34}$$

and the first two terms in (28):

$$\boldsymbol{u}^{\text{inc}}_0 = \left. \frac{\partial \left(\boldsymbol{u}^{\text{inc}}_{L(\text{plane})} + \boldsymbol{u}^{\text{ref}}_{L(\text{plane})} \right)}{\partial \vartheta_L} \right|_{\vartheta_L = 0}. \tag{35}$$

Differentiating (28) with respect to ϑ_L and using (35) we obtain

$$\left. \frac{\partial \boldsymbol{u}^{\text{tot}}_{L(\text{plane})}}{\partial \vartheta_L} \right|_{\vartheta_L = 0} = \boldsymbol{u}^{\text{inc}}_0 + \left. \frac{\partial \boldsymbol{u}^{\text{rem}}_{L(\text{plane})}}{\partial \vartheta_L} \right|_{\vartheta_L = 0}. \tag{36}$$

Since the differentiation symbols commute the left-hand side of (36) satisfies the equations of motion and the boundary conditions. Also, if an outgoing wave is differentiated with respect to ϑ_L the result is another outgoing wave. This differentiation does not change the nature of the corresponding tip condition either. It follows that $\partial \boldsymbol{u}^{\text{tot}}_{L(\text{plane})} / \partial \vartheta_L$ is the solution of the same wedge diffraction problem as $\boldsymbol{u}^{\text{tot}}_{L(\text{plane})}$ but under another incidence. Since the waves in $\partial \boldsymbol{u}^{\text{rem}}_{L(\text{plane})} / \partial \vartheta_L$ are outgoing, this incident field is $\boldsymbol{u}^{\text{inc}}_0$ and the left-hand side of (36) is $\boldsymbol{u}^{\text{tot}}_0$, the total field generated by the "creeping" wave incident on the wedge. We can now write

$$\boldsymbol{u}^{\text{tot}}_0 = \left. \frac{\partial \boldsymbol{u}^{\text{tot}}_{L(\text{plane})}}{\partial \vartheta_L} \right|_{\vartheta_L = 0} = \lim_{\vartheta_L \to 0} \frac{\boldsymbol{u}^{\text{tot}}_{L(\text{plane})}}{\vartheta_L}. \tag{37}$$

Eq. (37) suggests the following formula for calculation of the diffraction coefficients for the normalised "creeping" wave,

$$D_{0,\beta}(\vartheta) = \frac{\partial D_{L\beta}(0; \vartheta)}{\partial \vartheta_L} = \lim_{\vartheta_L \to 0} \frac{D_{L\beta}(\vartheta_L; \vartheta)}{\vartheta_L}. \tag{38}$$

Formulae (21) and (26) show that near the wedge tip the "creeping wave" has the amplitude $E_c (k_L d_0)^{-3/2}$, with d_0 defined graphically in Fig. 2. Therefore in order to calculate the diffraction coefficients $D^{\beta}_{T(\text{Gauss})}(\vartheta), \beta = L, T$ which are due to the transverse Gaussian beam incident at the critical angle we need to multiply (38) by this additional coefficient to get

$$D^{\beta}_{T(\text{Gauss})}(\vartheta) = \frac{E_c}{(k_L d_0)^{3/2}} D_{0,\beta}(\vartheta), \quad \beta = L, T \tag{39}$$

where we used the fact that in the far field $d_0 \approx \tilde{d}$.

The last formula suggests a limiting procedure that allows us to utilise the standard GTD to evaluate non-uniform asymptotics for the "creeping" wave diffracted off a planar faces crack. All we need to do given a wedge angle is to evaluate the standard diffraction coefficients using the existing numerical codes for a sequence of small incidence angles ϑ_L, each time dividing the result by the corresponding angle and multiplying by a constant and terminate the procedure on reaching a specified accuracy.

The resulting diffraction coefficients have singularities at the shadow boundaries associated with reflected waves as well as critical rays, where the non-uniform asymptotics are inapplicable. Similarly to the case of plane incidence [15] it is possible to introduce the uniform asymptotics that are valid inside penumbra associated with the Goodier-Bishop type waves as well as standard body waves. Moreover, the above considerations can be used to evaluate scattered head waves. We will discuss both topics in future publications.

5. Numerical results

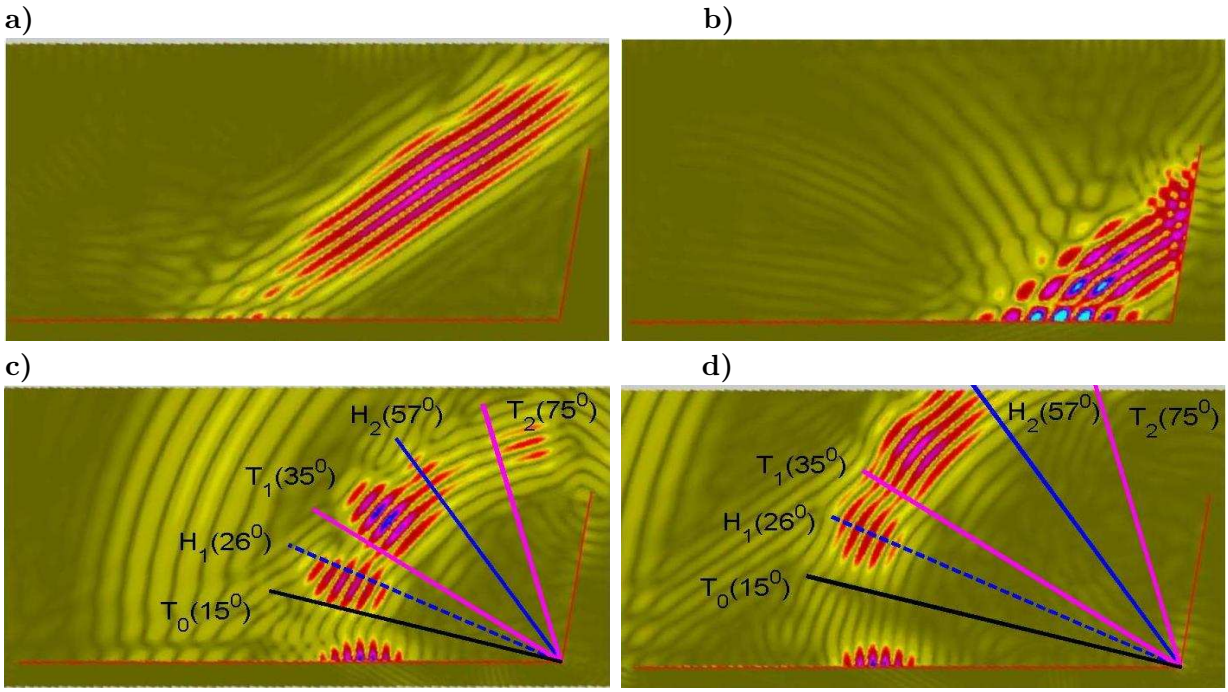

Figure 4. ATHENA simulations with a shear beam incident on the wall at the supercritical angle of 55^0. The crack angle is 100^0. The incident beam irradiates whole crack. a) and b) are consecutive snapshots of incident field. c) and d) are consecutive snapshots of scattered field.

Some features of the above models have been simulated numerically using ATHENA, a finite element commercial code. The simulation parameters are $c_L = 5890\,km/s$, $c_T = 3210\,km/s$ and the frequency is $2\,MHz$. We restrict all discussions to the surface-breaking crack which forms a 100^o angle with the back-wall and to the beam that is incident at 55^0 to this wall. In Figs. 4 - 6 we consider three different positions of the transducer as it moves away from the crack and study the changes in the respective scattered fields. Note that in ATHENA simulations it is assumed that the medium below the wall is air or water. For this reason non-zero displacements are indicated in Figs. 5 - 7 underneath the wall. The two consecutive screen shots presented in Fig. 4 a) and b) have been obtained for a transducer positioned so that when the beam hits the back-wall it irradiates the whole crack. The two consecutive screen shots presented in Fig. 6 a) and b) have been taken for a transducer moved so far from the crack that the beam hits the back-wall in front

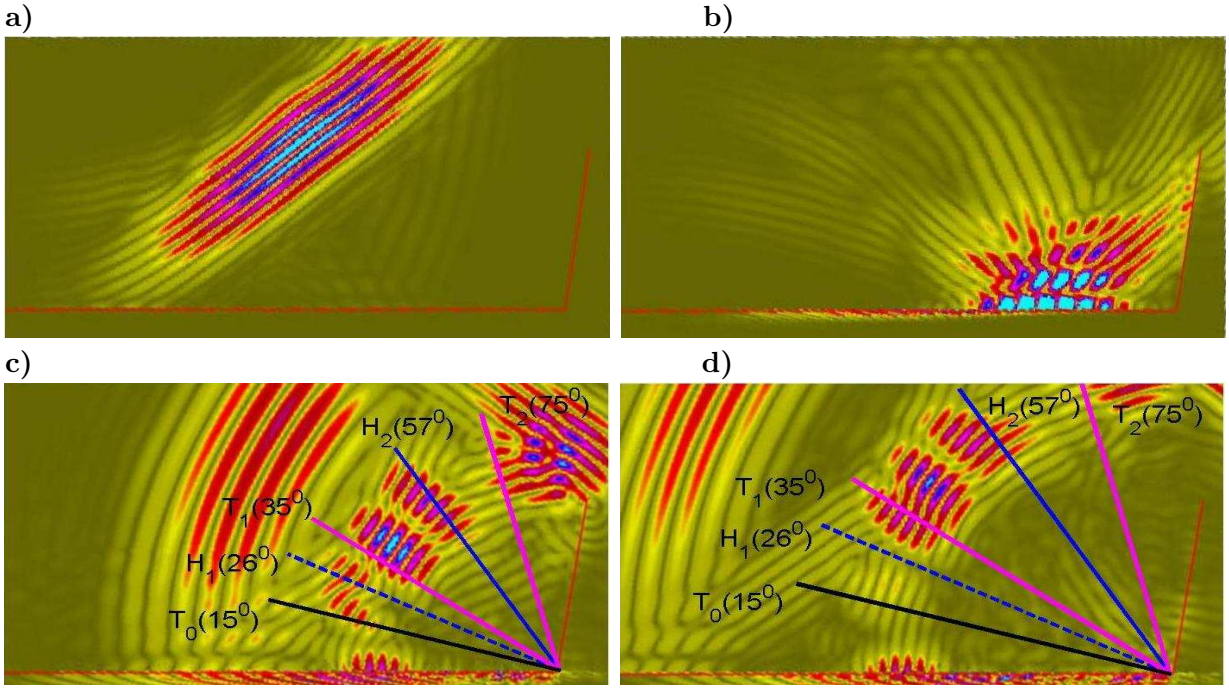

Figure 5. ATHENA simulations with a shear beam incident on the wall at the supercritical angle of 55^0. The crack angle is 100^0. A portion of the incident beam irradiates the crack. a) and b) are consecutive snapshots of incident field. c) and d) are consecutive snapshots of scattered field.

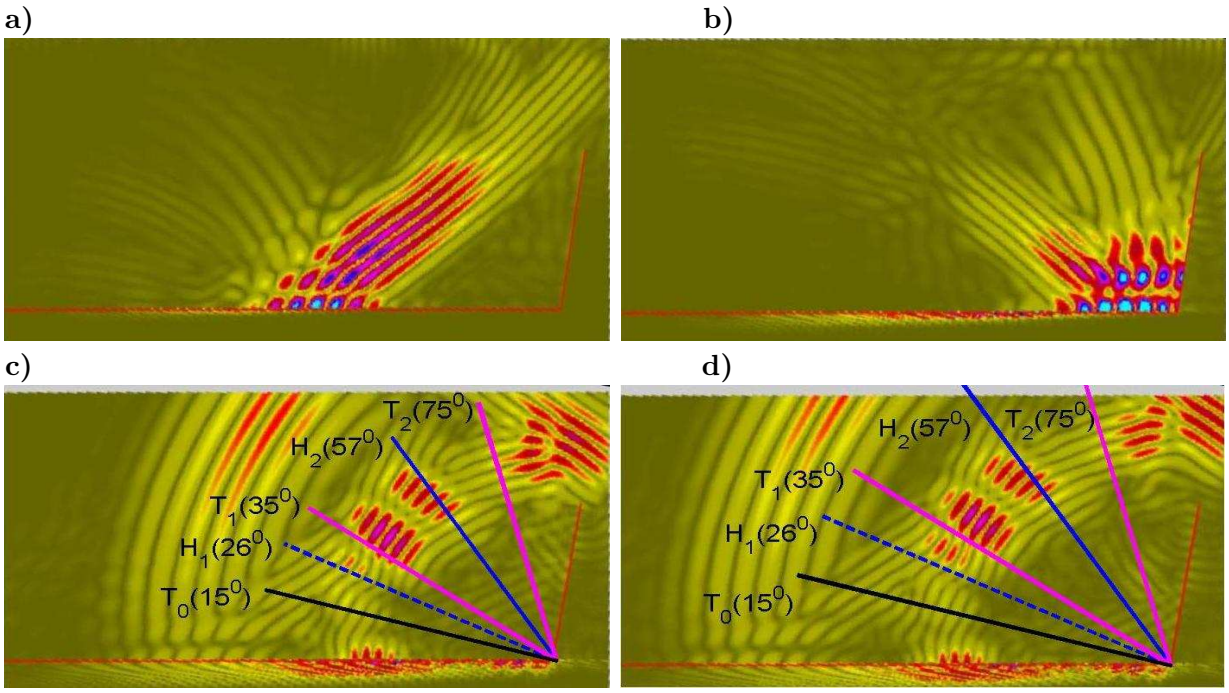

Figure 6. ATHENA simulations with a shear beam incident on the wall at the supercritical angle of 55^0. The crack angle is 100^0. The incident beam hits the wall in front of crack. a) and b) are consecutive snapshots of incident field. c) and d) are consecutive snapshots of scattered field.

of the crack and generates a "creeping" wave, which is the only wave that reaches the crack tip. Fig. 5 is an intermediate case and the two consecutive screen shots presented in a) and b) show

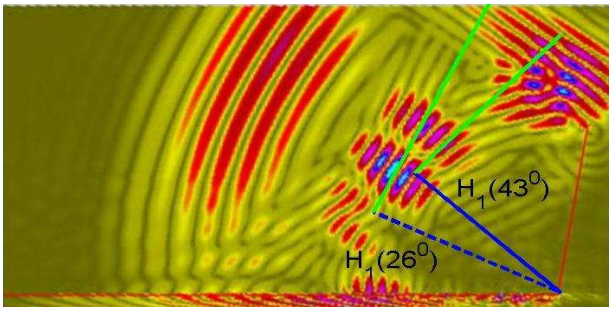

Figure 7. ATHENA simulations of the incidence of a shear beam at the supercritical angle of 55^0. The crack angle is 100^0. The incident beam irradiates the whole crack. Solid blue line - theoretical critical ray, solid green line - corresponding head wave front, Dashed green line - simulated head wave front, dahed blue line - corresponding critical ray.

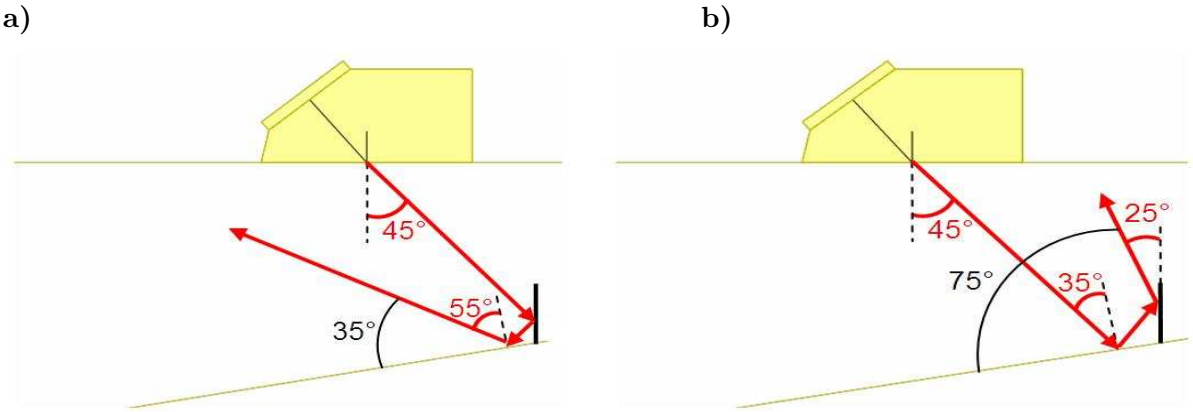

Figure 8. Geometry of two double reflected T waves.

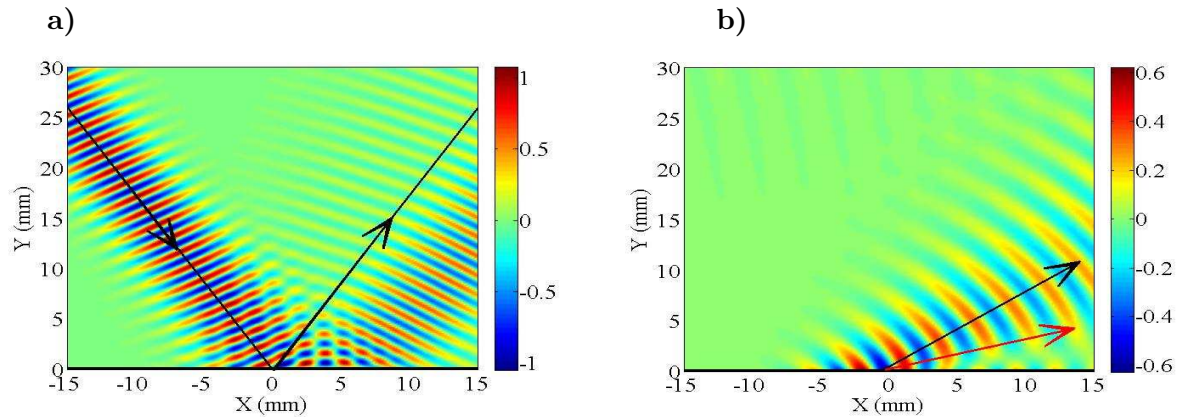

Figure 9. A Gaussian beam incident at the critical angle on a traction free surface. a) The transverse components of the incident and scattered fields. The black arrows indicate the direction of propagation. b) The longitudinal component of the scattered field. Black line - the direction of the scattered longitudinal beam $\approx 30^0$ to the back-wall. Red line - the direction of the scattered longitudinal lobe in [13]. Red line makes 16^0 with the back-wall.

that in this transducer position the crack is irradiated by both the "creeping" wave and a portion of the incident beam.

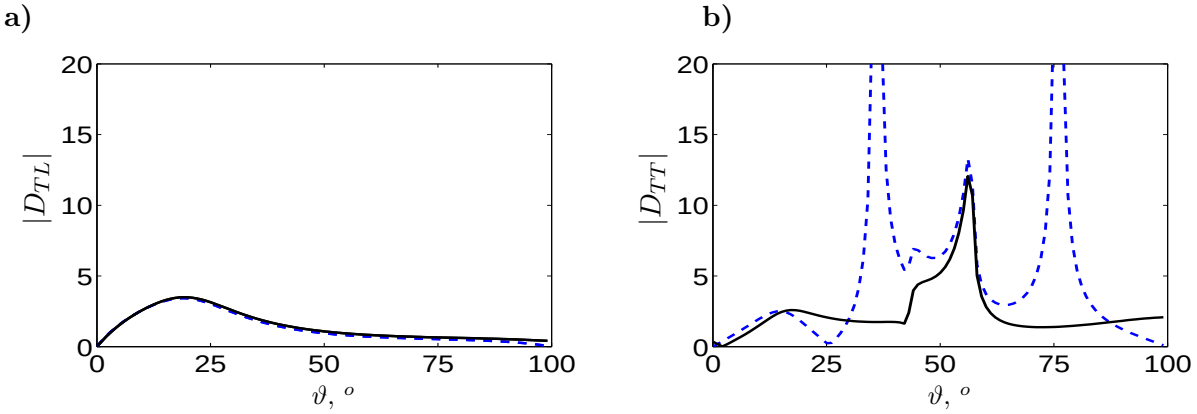

Figure 10. Diffraction coefficients vs the observation angle ϑ. The wedge angle - 100^0. The incident wave - the plane T wave incident at 56^0 to the wall (supercritical configuration). a) $D_{0,L}$ b) $D_{0,T}$. Dashed line - GTD coefficients, solid line - corrected coefficients as defined in [15].

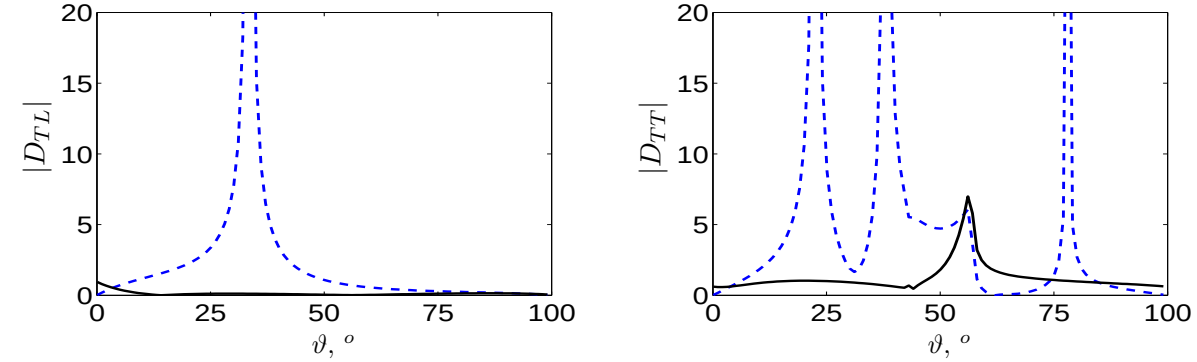

Figure 11. Diffraction coefficients vs the observation angle ϑ. The wedge angle - 100^0. The incident wave - the plane T wave incident at 58^0 to the wall (subcritical configuration). a) $D_{0,L}$ b) $D_{0,T}$. Dashed line - GTD coefficients, solid line - corrected coefficients as defined in [15].

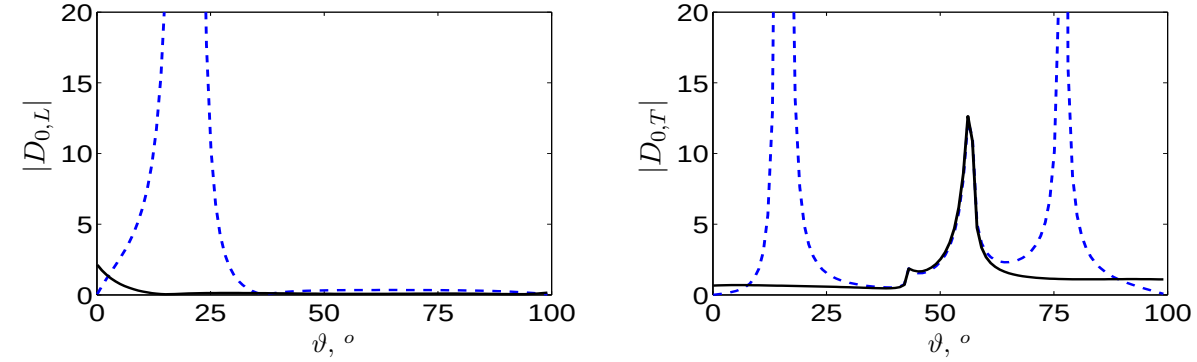

Figure 12. Diffraction coefficients vs the observation angle ϑ. The wedge angle - 100^0. The incident wave - the normalised creeping wave propagating along the wall. a) $D_{0,L}$ b) $D_{0,T}$. Dashed line - GTD coefficients, solid line - corrected coefficients as defined in [15].

Let us first discuss geometry of the resulting scattered fields presented in c) and d) portions of Figs. 4 - 6. They all feature two circular wave fronts, T and L, centered at the crack corner as well as the corresponding head wave fronts as well as the following T rays,

- T_0 (at 15^0 to the wall) - the T reflection of the L component of the wall creeping wave,
- T_1 (at 35^0 to the wall) - the shadow boundary associated with the twice reflected T wave,
- H_1 (at 26^0 to the wall) - the critical ray associated with the diffracted head wave,
- H_2 (at 57^0 to the wall) - the critical ray associated with the diffracted head wave,
- T_2 (at 75^0 to the wall) - the shadow boundary associated with the twice reflected T wave.

The angles of propagation of the waves T_1 and T_2 are justified by reference to Figs. 8 a) and b), respectively. The angle of propagation of T_0, the T reflection of the L portion of the creeping wave is found using the Snell's law. The situation with the head waves is more complicated: had the vertical crack face been of infinite extent the critical rays would each form $\cos^{-1}(\gamma) \approx 57^0$ with the corresponding crack face. In the ATHENA simulations presented in Figs. 4 - 6, the critical ray H_2 corresponding to the lower head wave front indeed appears to run at $\approx 57^0$ to the back-wall. However, the upper head wave front in these simulations is inclined at such an angle that the corresponding critical ray H_1 runs at 26^0 to the back-wall rather than 43^0 - see Fig. 7. This might be due to the fact simulations have been carried out for a finite crack. Indeed, the problem is less pronounced in simulations involving larger cracks. To indicate the tentative nature of the ray H_1 it is depicted in Figs. 4 - 6 using the dashed line. Let us proceed with our comparisons. In accordance with Fig. 8, both T_1 and T_2 singularities at about 35^0 and 75^0, respectively, are present in Figs. 10b) and 11b). When the incident beam hits the back-wall before the crack, the creeping diffraction coefficient in Fig. 12b) lacks the T_1 singularity, because in this configuration there can be no rays shown in Fig. 8a). Moving on to the T_0 wave, when the incident beam irradiates the whole crack, we can apply the canonical model of diffraction of plane incident wave. If the angle of incidence is smaller (greater) than $\cos^{-1}(\gamma)$, the configuration is supercritical (subcritical) and we do not have (have) a body L wave incident on the vertical crack face. This explains why there is a singularity at about 18^0 in the standard T GTD diffraction coefficients presented in Fig. 11b) but there is no such singularity in Fig. 10b). When the incident beam hits the back-wall before the crack, the creeping diffraction coefficient in Fig. 12b) has the corresponding singularity at about 15^0. There is a difference between the nature of these singularities: it has been established numerically that in Fig. 10b) we have a single pole at 20^0 and in Fig. 12, the T_0 singularity at 15^0 is a double pole. The latter behaviour is characteristic of the Goodier-Bishop wave. For similar reasons, there a single pole at about 20^0 in the standard L GTD diffraction coefficients presented in Fig. 11a), there is no such singularity in Fig. 10a) and in Fig. 12a) the singularity at 20^0 is a double pole. Note that the corrected diffraction coefficients presented in Figs. 10) - 11 are calculated using the standard recipe described e.g. in [15].

Let us now study the energy variation in the scattered fields as presented in c) and d) parts of Figs. 4 - 6. The comparison is complicated by the difference in amplitude scaling, since in Fig. 5 the incident amplitude appears to be much stronger than in other configurations. It is important to keep in mind that in the ATHENA simulations supercritical incidence was used and thus the situation corresponds to Fig. 10 rather than Fig. 11. To start with, all scattered fields contain the Rayleigh wave travelling along the back-wall. According to Figs. 10a) and 12a), the diffracted L waves are supposed to be very weak. The fact that we see high intensity patches superimposed on the L fronts in Figs. 5c) and d) and Figs. 6c) and d) must be due to the reflection at the vertical crack face of the L component of the creeping wave. Note that there is no high intensity region superimposed on the L front in Figs. 4. This is consistent with the fact that in this supercritical configuration no L wave is incident on the vertical crack face. We now turn attention to the lowest bright spot seen on the T fronts in Figs. 4c) and d). It is natural to assume that it is due to T_1. Indeed, in accordance with Fig. 8b) it appears beneath the shadow boundary running from the crack corner at 35^0 to the back-wall. In Figs. 5c) and d) the corresponding spot is much weaker, which is consistent with the fact that in this configuration the crack is only partially irradiated by the incident beam. However, there are many problems associated with this hypothesis. The ATHENA simulations are more consistent with the idea that the spot is due to interference between T_0 and T_1. This would explain why the spot is not touching the 35^0 ray in

Fig. 4c) and why it is closer to it in Figs. 4d). Furthermore, the new hypothesis would explain why the shift is even stronger in Fig. 5 and why it is accompanied by increase in amplitude. Indeed, in this case the contribution of the T_1 wave is much weaker than when the whole of the crack is irradiated and T_0 has a Goodier-Bishop component whose amplitude increases in a linear fashion in the direction normal to the direction of propagation. The hypothesis also accounts for the weak spot associated with the corresponding ray in Fig. 6c): in this case the T_1 wave is particularly weak, because it is generated by the weak outer beam margin hitting the crack's vertical face. Again, the intensity of the spot grows with time from Fig. 6c) to Fig. 6d), which is hard to explain for any wave other than the Goodier-Bishop type. The fact that this spot is so much brighter in Fig. 5c) than in Fig. 6c) must be partly due to the difference in the incident amplitude.

Moving in the clockwise direction along the circular T front, the other two bright spots in the scattered fields, which sometimes coalesce and which are present in all three figures, must be due to two head waves, H_1 and H_2. The spots lie inside the intersection of both corresponding irradiated zones. The third bright spot present in all figures is easily assigned to the T_2 wave, since it lies just above the 75^0-ray which is, according to Fig. 8b), the T_2 irradiated zone. Other bright regions above this spot are due partly to waves diffracted by the top crack tip and mainly to the single reflection at the back-wall of the incident beam.

We finish this section by the stationary simulation of scatter of a Gaussian beam incident at the critical angle by the traction free interface. It is obtained by applying the inverse Fourier transform to (16) and numerical evaluation of the resulting integrals (Fig. 9). The black arrowed lines in Fig. 9a) indicate the axis of the incident beam and its geometrical optics (GO) reflection. The reflected beam itself demonstrates a well-known lateral shift from the GO path [10]. Fig. 9b) presents the reflected L component. The black line in Fig. 9b) indicates the direction of the main beam propagation, which makes approximately 30^0 with the back-wall.

6. Discussions

There are many controversies surrounding grazing incidence and creeping wave. To start with, because in this limit the incident and reflected L waves coalesce, neither Kirchhoff approximation nor uniform asymptotics of incident and scattered fields taken when in isolation extend to grazing incidence. The solution lies in decomposing the total field into a sum of the grazing waves (incident and reflected plane waves - in the regions where they exist) and the waves diffracted by the crack edge - see in [11], [9] and references therein. When seeking asymptotics, the procedure should be carried out for the incidence angles which are close to grazing and then utilising a limiting procedure. When the limiting incident wave is of the Goodier-Bishop type this should be based on (37). Otherwise, one should just employ continuity considerations [9]. Though arising from mathematical considerations the Goodier-Bishop waves vex many physicists (e.g. [8]). A particular problem arises when the incident wave is plane and transversal, propagating at a critical angle to the surface. In this case the problem is ill-posed. However, no issue surrounds the Goodier-Bishop type waves arising in the problem considered in this paper, because they only figure only in a near boundary approximation. Finally, the term "creeping" wave as used in engineering literature deviates from the accepted usage in applied mathematics. In applied mathematics a creeping wave is a single wave gliding along a curved surface and decaying exponentially (see [12] and references therein). For this reason, some authors - see e.g. [13] - question the existence of a creeping wave in the configuration considered above. In principle, their conclusion is similar to ours: under a critical incidence there arises a disturbance near the boundary which looks like a creeping wave, but is in fact a combination of well known body waves which decays away from its source as $(k_L R)^{-3/2}$. With reference to Fig. 9, the illusion of a surface wave arises at distances from the specular point $(0, 0)$ which are smaller than 10 mm. This corresponds to distances observed in Figs. 4 - 6. Note that when the "creeping" wave hits the crack, apart from exciting diffracted waves each of its components reflects according to the Snell's law. However it is possible to say that the incident "creeping" wave generates reflected and transmitted "creeping" waves [14]. The situation is not identical to the Rayleigh wave incidence, because unlike in the latter case, the

interaction between the "creeping" wave and the crack leads to reflected T and L waves as well.

7. Conclusions

In this paper we have studied interaction of a shear Gaussian beam with a back-wall crack. It has been shown that when the incidence is near critical the Gaussian beam excites a strong "creeping" wave which soon attenuates. This "creeping" wave has a T component (the head wave) and L component which - in the near boundary approximation - comprises the plane surface wave and a Goodier-Bishop type wave. We have presented a method for evaluating the diffracted field when the wedge is irradiated by the "creeping" wave and calculated the resulting diffraction coefficients. The full uniform description of the scattered field will be the subject of future investigation.

8. Acknowledgement

This work has been carried out within the framework of the CIVAMONT 2012 collaborative project.

References

[1] Achenbach A, Gautesen A, and McMaken H 1979 *Ray Methods for Waves in Elastic Solids; With Applications to Scattering by Cracks* (New York: Pitman)
[2] Kamotski V, Fradkin L, Babich V M, Borovikov V A, and Samokish B A 2006 *SIAM J. Appl. Math.* **67**(1) 235
[3] Gautesen A and Fradkin L 2011 *SIAM J. Appl. Math.* **70**(8) 3065
[4] Goodier J N and Bishop R E D 1952 *J. Appl. Phys.* **23**(1) 124
[5] Cerveny V and Ravindra R 1971 *Theory of Seismic Head Waves* (Toronto: University of Toronto Press)
[6] Bleistein N and Handelsman R A 1986 *Asymptotic Expansions of Integrals* (New York: Dover)
[7] Borovikov V A 1994 *Uniform Stationary Phase Method* (London: IEE)
[8] Graff K F 1975 *Wave Motion in Elastic Solids* (London: Oxford University Press)
[9] Thomson I 2006 *Proc. R. Soc. A* **462** 1341
[10] Pott J and Harris J G 1984 *J. Acoust. Soc. Am.* **76**(S1) S64
[11] Ufimtsev P Ya 2007 *Fundamentals of the Physical Theory of Diffraction* (Chicester: Wiley-Blackwell)
[12] Tew R H, Chapman S J, King J R, Ockendon J R, Smith B J and I Zafarullah 2000 *Wave Motion* **32** 363
[13] Langerberg K J, Fellinger P and Marklein R 1990 *Res. Nondestr. Eval.* **2** 59
[14] Huet G, Darmon M, Lhemery A and Mahaut S 2009 *Springer Proc. Phys.* **128** 217
[15] Zernov V, Fradkin L and Darmon M 2011 *J. Phys.: Conf. Series* this issue